Eur. Phys. J. Plus (2024) 139:901
https://doi.org/10.1140/epjp/s13360-024-05644-8

THE EUROPEAN PHYSICAL JOURNAL PLUS

Regular Article

Thermal cross section of poly(2-hydroxyethyl methacrylate) hydrogels for neutron dose calculation

Margherita Simoni[1], Carla Andreani[1,2], Laura Fazi[1], Emiliano Fratini[3], Teresa Guaragnone[3], Matthew Krzystyniak[4], Anna Prioriello[1], Roberto Senesi[1,5], Giovanni Romanelli[1,4,a]

[1] Department of Physics and NAST Centre, Universitá degli Studi di Roma Tor Vergata, 00133 Rome, Italy
[2] National Research Council, Institute of Polymers, Composites and Biomaterials (IPCB), 80078 Naples, Italy
[3] Department of Chemistry "Ugo Schiff" & Center for Colloid and Surface Science (CSGI), University of Florence, Via Della Lastruccia, 3, 50019 Firenze, Italy
[4] ISIS Neutron and Muon Source, Rutherford Appleton Laboratory, Chilton OX110QX, UK
[5] CNR-ISM, Via del Fosso del Cavaliere 100, 00133 Rome, Italy

Received: 25 March 2024 / Accepted: 11 September 2024

Abstract Phantom materials are used to design radiation safety and protection strategies by means of numerical dose calculation. In the case of thermal neutrons, the radiation transport in the phantom relies on mass attenuation coefficients and total cross sections which are dependent on the physical and chemical properties of the material. Specifically for medical applications, such as neutron capture therapy, the neutron-induced dose is mainly related to the neutron absorption by hydrogen and nitrogen in the human tissue and body. Here, we investigate the use of poly(2-hydroxyethyl methacrylate) as a phantom material by experimental measurement and modeling of its total neutron scattering cross section and mass attenuation coefficient. We show that by varying the hydration level from 10 to 40 w%, one can obtain a neutron attenuation coefficient similar to polymethyl methacrylate or more representative of the human body, respectively. By benchmarking our phenomenological model on the experimental data, we provide a new example of how to use the average functional group approximation to accurately model total neutron cross sections in the framework of personalized medicine approaches.

1 Introduction

Neutron capture therapy is an oncologic treatment that employs an epithermal neutron beam to irradiate the cancer region, making use of suitable drugs that are selectively delivered to the tumor [1]. These drugs are often rich in boron, specifically in ^{10}B , an isotope with a high neutron absorption cross section. The technique takes advantage of the energetic ions produced by the neutron capture reaction $^{10}\mathrm{B}\,(\,\mathrm{n}\,,\,\alpha)^{7}\mathrm{Li}$, which are able to deliver a large amount of energy over small regions of a few micrometers, therefore destroying cancer cells without affecting healthy ones. To employ this technique in clinical applications, it is essential to estimate the total dose delivered, in order to maximize it on the cancer region and reduce it on the healthy tissue. To obtain clinically relevant dosimetric information, it is important to characterize the neutron beam and have a good understanding of neutron transport inside soft tissue. Epithermal neutron beams (0.5–10 keV) are employed for medical treatment. In the epithermal energy range, neutrons are not easily absorbed and interact mainly through proton recoil processes. When they enter the body, epithermal neutrons are again moderated by interacting with the soft tissue. Their initial energy is chosen so that when they arrive at the tumor position, they are in the thermal energy range and are easily absorbed by the boron deposited in the growth. However, thermal neutrons can also be absorbed by other elements that are abundant in the human body. The elements with the highest neutron absorption cross sections that are also abundant in the human body are hydrogen and nitrogen, which produce ions and γ-rays through the reactions $^{14}\mathrm{N}\,(n,\,p)^{14}\mathrm{C}$ (ca. 1.9 barn at 25 meV) and $^{1}\mathrm{H}\,(n,\,\gamma)^{2}\mathrm{H}$ (ca. 0.3 barn at 25 meV), thus delivering an undesired dose to the patient. The total absorbed dose on the tissue is given by the contribution of not only epithermal neutrons but also thermal neutrons originated by moderation, a variety of secondary particles, γ-rays—both present in the beam and generated by absorption reactions—and fast neutrons that weren't correctly moderated.

The cross section in the range of fast neutrons depends mainly on the stoichiometry of the system and only slightly on the chemical interactions between the atoms. Therefore, it can be well approximated by the sum of the cross section contributions of different atoms, allowing for accurate transport simulations using Monte Carlo codes. On the other hand, the thermal and epithermal

Guest editors: A. Malizia, M. D'Arienzo, G. M. Contessa, F. d'Errico, S. De Souza Lalic, F. Duschek, V. Vasiliou, T. Hooker, P. Gaudio.

[a] e-mail: giovanni.romanelli@uniroma2.it (corresponding author)

Published online: 17 October 2024

neutron cross sections are greatly affected by the chemical and structural properties of the material and by the relative concentration of the main absorbers and scatterers (such as hydrogen and nitrogen). Simulating complex organic molecules is a complicated and time-consuming task, and therefore, neutron transport codes in the range of thermal neutrons currently rely on neutron libraries, which are only available for a handful of materials. The use of simplified materials as phantoms can bring to approximations in the calculation of the dose when compared to the complex molecular systems in the human body. Recently, an approximation was proposed [2] that allows accurate prediction of the thermal scattering cross sections of hydrogenated materials, referred to as the Average Functional Group Approximation (AFGA). This method, if validated under clinically relevant conditions, could allow the simulation of the transport of neutrons inside different body parts of a patient. Together with other experimental techniques that measure the abundances of hydrogen-containing functional groups, the transport codes based on AFGA could contribute to developing a "personalized medicine" approach to BNCT. The validation of transport codes for clinical use requires the comparison between measured and modeled fluence rate and dose distribution. These measurements rely on the use of phantoms, which are chosen to approximate the chemical composition of the human body.

Clinical dosimetry often employs phantoms to characterize the absorbed dose distribution and the neutron fluence rate, both for beam calibration and for the validation of transport simulations [3, 4]. Measuring the dose of a well-known phantom is the first step necessary to clinical dosimetry to relate the beam parameters to the actual dose delivered to the body. Phantoms are, therefore, made of well-characterized materials that roughly approximate the human body with respect to the radiation of interest. Contrary to charged particles and photons, which are sensitive to the elemental stoichiometry and density of the material, neutron transport is also strongly affected by chemical interactions, rendering it necessary for the phantom to reflect the chemical complexity of the human body. Historically, the most used phantom materials have been water and PMMA (polymethyl methacrylate). The use of water as a phantom, especially in neutron dosimetry, represents a substantial oversimplification, but it is incredibly popular because it portrays the high content of water in soft tissue while being a practical and easily reproducible solution, some examples of the applications of water phantoms include those in Refs. [4–6]. In the field of liquid phantoms, some liquid tissue equivalent (TE) materials have been proposed for dosimetry measurements. Tissue equivalent compounds are defined to match the average stoichiometry of an organ without reproducing the complex molecules that compose it. Therefore, they are particularly useful in dosimetry measurements of photons, electrons, and even charged hadrons radiation, as well as fast and epithermal neutrons, but they still grossly simplify the transport of thermal neutrons inside the human body. Raaijmakers et al. [7] analyzed a TE liquid that well represents muscle tissue, defined by the International Commission on Radiation Units & Measurements (ICRU) as the "Goodman liquid" in the ICRU 44 [8], but they did not find particular advantages to this material for neutron dosimetry applications compared to classical water phantoms. Similarly, Eppala et al. [9] compared water to two other TE liquids defined by them to agree with the ICRU 44 standards for brain tissue. They concluded that water is a suitable brain tissue substitute for periodic calibration and quality control; while, tissue equivalent liquids could be considered when higher accuracy is required by the specific application. Therefore, they still identify water as a reference liquid material for practical reasons.

The most used solid material for phantom applications is PMMA, a widely-produced polymer that is both cheap and well-suited to approximate the human body compared to other popular polymers. PMMA was first suggested as a reliable water substitute by the International Atomic Energy Agency (IAEA) in 2000 for electron beam and X-ray dosimetry. This material, composed of hydrogen, carbon and oxygen atoms, presents a greater chemical diversity compared to polymers like Polypropylene or Polystyrene and a hydrogen content more similar to that of the human body compared to polymers like Polycarbonate or Polyethylene, as well as Polypropylene and Polystyrene. As an example, it has been shown that the fluence rate and delivered dose in Polyethylene differ by more than 30% from that of water at a 2 cm depth; while, the absolute dose delivered by neutrons agreed within 3% for water, PMMA and the muscle equivalent liquid mentioned before [7]. However, the dose delivered by secondary particles, produced when thermal neutrons are absorbed, is still underestimated in PMMA because of the absence of nitrogen and lower hydrogen concentration. It is important to note that although the presence of nitrogen in the human body significantly contributes to the total thermal neutron absorption cross section, PMMA is preferred to polymers like Nylon, for which the nitrogen content is too high to represent soft tissues. Similarly, polymers containing other non-abundant elements are not preferable as phantom materials. These characteristics have contributed to the popularity of PMMA in the field of phantom materials, not only for neutron radiation. In the case of neutron dosimetry, multiple calibration and characterization measurements for the neutron source instrumentation have been performed using PMMA phantoms, both as bulk phantoms [3, 10–13] or as containers for a water phantom [4]. The choice of combining water and PMMA phantoms can be attributed to the low hydrogen content of PMMA, compared to soft tissue, which contributes to over-estimate neutron fluence and under-estimate γ-ray dose induced neutron absorption [7]. Similarly to TE liquids, it is possible to define TE solid materials that can be compared to PMMA performances. In TE materials, carbon atoms are sometimes substituted with oxygen atoms to obtain a stable and electrically conductive material that can be used as an electrode in dosimetry devices; while, their hydrogen and nitrogen compositions are chosen to match those of the soft tissue they aim to approximate. Two examples of this are A150 [14] and A181 TE plastic [15] formulated to represent muscle tissue and brain tissue, respectively. Other solid tissue equivalent materials such as solid water [16] have been suggested as solid TE materials, but while they may reproduce more accurately organic tissues, PMMA still appears to be the most practical solution for solid phantoms.

Here, we investigate the potential use of hydrogel materials such as Poly(2-hydroxyethyl methacrylate) (pHEMA) as an alternative to the most commonly used phantom materials and present transmission experiments to validate the modeling of its thermal neutron cross section using AFGA. This will be a first step to better reproduce both the chemical diversity and high-water concentration of

the human body. In particular, experiments and modeling were performed on pHEMA in the form of a hydrogel in a range of water contents up to 40 w% of its mass.

2 Materials and methods

Poly(2-hydroxyethyl methacrylate) (pHEMA) was synthesized using the materials and methods described in the following sections. This polymer forms a hydrogel when hydrated. Four different samples were prepared with different levels of hydration, which were chosen to be of 10 w%, 20 w%, 30 w% and 40 w% of the mass of the hydrogel, respectively. The hydrogel samples were prepared with a thickness of about 2 mm in order to guarantee optimal neutron transmission measurements. Each sample was enclosed inside a hermetic LDPE bag to preserve the correct hydration. Each LDPE bag had a thickness significantly smaller than that of the pHEMA sample (ca. 0.2 mm) to guarantee minimum contribution to the cross section.

2.1 Materials

2-Hydroxyethyl methacrylate (HEMA) (CAS: 868-77-9, assay 97%) and ethylene glycol dimethacrylate (EGDMA) (CAS: 335681, assay $\geq$ 98 %) were obtained from Merck and were used as received. Water was purified by a Millipore MilliRO-6 Milli-Q gradient system (resistivity > 18 M Ω cm). pHEMA hydrogels were prepared by mixing HEMA monomer and EGDMA crosslinker. The solution was bubbled for 1 min to remove dissolved oxygen that could inhibit the polymerization reaction. Afterward, α,α'-Azoisobutyronitrile (AIBN) initiator (CAS: 78-67-1, assay 98%) and water previously degassed were sequentially added. The mixture was transferred between two glass windows and reacted at $60°C$ for 4 h. The obtained flat transparent hydrogel, with a teflon spacer of 2 mm in thickness, was washed in fresh water and renewed once a day for 7 days to remove unreacted monomers. pHEMA hydrogels with 10 w%, 20 w%, and 30 w% hydration levels were obtained by dehydrating the 40 w% system. Pieces of gels were cut ($5 \times 5 \times 0.2$ cm^3) and placed into controlled humidity chambers with 75% and 94% r.h., using saturated solutions of sodium chloride and potassium nitrate, respectively. The weight of the hydrogels was monitored until it reached a steady value. The equilibrium water content was calculated as follows:

$$\%\text{water} = \frac{W_i - W_d}{W_i} \tag{1}$$

where W_i is the weight of the sample at day i and W_d the weight of the dry sample. The values of W_d are experimentally determined from TGA analysis.

2.2 Neutron transmission

Neutron transmission experiments were conducted on the VESUVIO beamline [17–19] at the ISIS Neutron and Muon Source. Measurements were performed using the time of flight (ToF) technique to obtain the neutron transmission as a function of the incident neutron energy in the range of 1 meV-1 keV. The VESUVIO transmission detector is a glass scintillator, specifically a GS20, which is enriched with 95% of lithium-6 (7.33 w%). The GS20 measures the flux of incoming neutrons, as well as the time of arrival on the detector, to obtain the energy dependence with ToF. The distances between the VESUVIO water moderator and the detector were calibrated as in [20]. Once the instrument is calibrated, it is possible to easily handle the conversion from ToF to neutron energy within the MANTID environment [21]. The sealed samples were then enclosed into flat aluminum containers that make a negligible contribution to the transmission measurements because of their thickness, as well as the low scattering cross section of the aluminum. In order to obtain the transmission contribution of the hydrated polymer alone, additional transmission spectra were acquired, portraying only the aluminum sample holder and the LDPE bag. These spectra were subtracted from the hydrated polymer spectra within the MANTID environment. From transmission data, it is possible to derive the macroscopic cross section (also known as neutron removal cross section) of the sample, employing the Beer–Lambert law:

$$T = e^{-\sum_i n_i \sigma_i t} \tag{2}$$

Therefore, applying the negative logarithm of the transmission, it is possible to obtain a spectrum that is proportional to the cross section, sometimes referred to as scattering power. In order to report the cross section in units of barn, the spectra were normalized so that their high energy limit would tend to the σ_{free} limit. To do so, the spectra were fitted with a function that follows the trend of the Short-Collision-Time Approximation (SCTA):

$$\sigma(E) = \sigma_{\text{free}}\left(1 + \frac{k_B T_{\text{eff}}}{2AE} + O(E^{-3})\right) \tag{3}$$

with:

$$\sigma_{\text{free}} = \sigma_{\text{bound}}\left(\frac{A}{A+1}\right)^2 \tag{4}$$

where σ_{bound} is the bound scattering cross section [22]. The function for $\sigma(E)$ approximates at high energies the cross section of a single nucleus with mass number A. Even though our system is composed of multiple nuclei, it is possible to fit data in the high energy limit with a function that follows the same trend but is proportional to the σ_{free} of the whole system:

$$\sigma(E) \simeq \sigma_{\text{free}}\alpha\left(1+\frac{\beta}{E}\right) \tag{5}$$

If the chosen energy range guarantees the validity of the approximation and if the function is correctly normalized to σ_{free}, the parameter α should be equal to 1. Otherwise, it is possible to scale data to impose $\alpha = 1$. Data can also be represented in terms of the mass attenuation coefficient $\Sigma(E)/\rho$, where $\Sigma(E)$ is the macroscopic cross section and ρ the density of the system. In this case, the Beer–Lambert law becomes:

$$T = e^{-\Sigma t} = e^{-\rho\left(\frac{\Sigma(E)}{\rho}\right)t} \tag{6}$$

Expressing the transmission in terms of $\Sigma(E)$ allows one to extrapolate easily the percentage of transmitted neutrons at a certain depth t. However, a precise measure of the density of the sample is not always known and may vary within the sample. The mass attenuation coefficient $\Sigma(E)/\rho$, on the other hand, can be obtained knowing the cross section $\sigma_i(E)$ of the constituent i, its molecular mass m_i, and the mass percentage of the molecules, as in:

$$\left(\frac{\Sigma(E)}{\rho}\right) = \sum_i \frac{\rho_i}{\rho}\left(\frac{\Sigma(E)}{\rho}\right)_i = \sum_i \frac{\rho_i}{\rho}\left(\frac{\sigma_i(E)N_A}{m_i}\right) \tag{7}$$

One can, therefore, scale the microscopic cross section of the sample to obtain a macroscopic mass attenuation coefficient without the need for a precise measurement of the density.

2.3 Average functional group approximation

The AFGA approach [2] is based on the fact that hydrogen greatly contributes to the thermal scattering cross section of organic materials. Hydrogen contribution to the incoherent cross section of a polymer is particularly significant because this atom has the highest incoherent cross section compared to any other element. This makes the incoherent approximation particularly suitable to describe hydrogen-rich materials (such as polymers). Moreover, its mass is close to that of neutrons; and therefore, it exchanges with neutrons a higher amount of energy compared to any other atom, easily thermalizing them. For these reasons, it is possible to rationalize a polymer as composed of hydrogen atoms that belong to specific functional groups. The AFGA consists of approximating the total incoherent scattering cross section of a polymer using the contribution of each functional group that composes the polymer. The purpose of this approximation is to provide a simplified and phenomenological method to estimate the thermal neutron cross section of polymers and organic molecules, which could render unnecessary more complex atomistic simulations. It is also important to notice that experimental data of thermal neutron cross sections are not available for many materials, thus rendering this approximation particularly useful in the analysis of complex compounds. AFGA can therefore be implemented to investigate 3D-printed instrument components [23], neutron moderators or shielding materials in order to compare different recipes and predict how the neutrons interact with them. Moreover, it can be employed for the transport codes used in neutron capture therapy to simulate neutron interaction with different organs, tissues or drugs [24].

AFGA calculations of the scattering cross sections run within the NCrystal environment [25] and are based on the formalism reported in ref. [2]. The AFGA cross section of the hydrated pHEMA polymer was here calculated using the NCrystal cross section of liquid H_2O obtained in refs. [26–30]. The stoichiometry was defined according to the levels of hydration chosen for the experimental samples to obtain four different theoretical cross sections that differ for the water content.

Figure 1 shows the comparison of the scattering cross section of pHEMA, as calculated using AFGA, and water, from the CAB model by Marquez-Damian et al. [26–30], both as normalized to unity for epithermal neutrons (left) and as mass attenuation cross section, i.e., the attenuation coefficient for unit mass density (right). The left panel shows how both cross sections feature a change of slope, whose position approximately depends on the separation between lattice and internal vibrational modes in each molecular system. In the case of water, the cross section features a change of slope at about 70 meV, where neutrons can start to interact inelastically with the molecule by exciting librational modes, while at lower energies, they can only interact with the diffusion and translational modes. In the case of pHEMA, the change in slope occurs at higher energies, about 150 meV. The vibrational density of states of a polymer, compared to that of a small molecule such as water, is quite rich in the region of the lattice modes, and the separation between local/internal vibrations and lattice modes becomes somewhat arbitrary. However, one can expect that the latter case is much more representative of the hydrogen dynamics in the human body and tissue, as opposed to the case of liquid water.

The right panel of Fig. 1 shows the mass attenuation factor of the two molecular systems. These functions are more representative of the different attenuation properties of the two systems, which have an impact on the calculation of the neutron moderation within the material and the resulting dose released therein, as they depend on the monomer/molecule mass and stoichiometry. As will be discussed shortly, by synthesizing pHEMA samples at different hydration levels, the attenuation coefficient of the dehydrated polymer can be slightly increased with respect to dehydrated pHEMA and fine-tuned to be more representative of the human body.

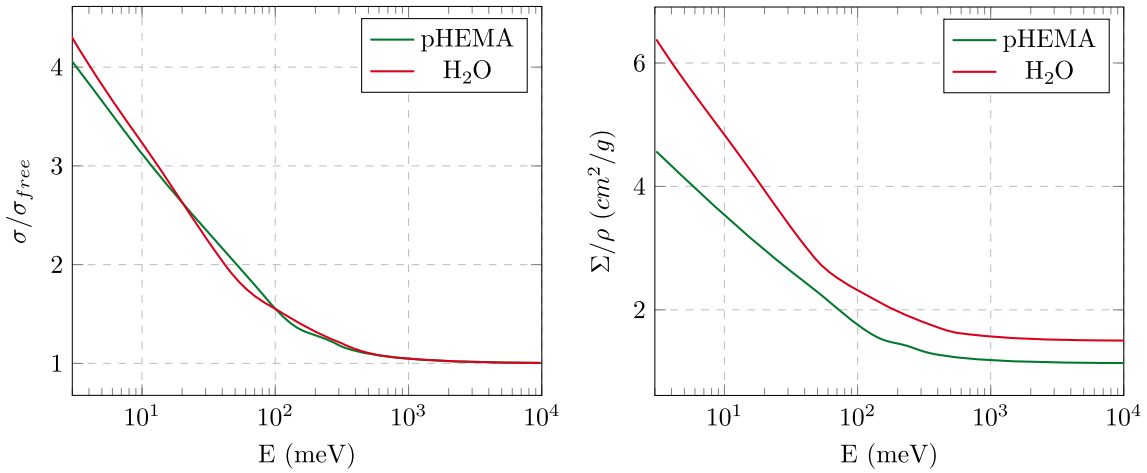

Fig. 1 Calculated scattering and attenuation properties of water and pHEMA as total scattering cross section normalized to the free cross section for epithermal neutrons (left panel) and as mass attenuation factor (right panel) as a function of the incident neutron energy. It can be noted that the error bars are smaller in the central region, this is due to the H_2O moderator, which thermalizes neutrons so that the their distribution has a peak around $\frac{3}{2}K_BT$, making neutron flux higher in that energy region

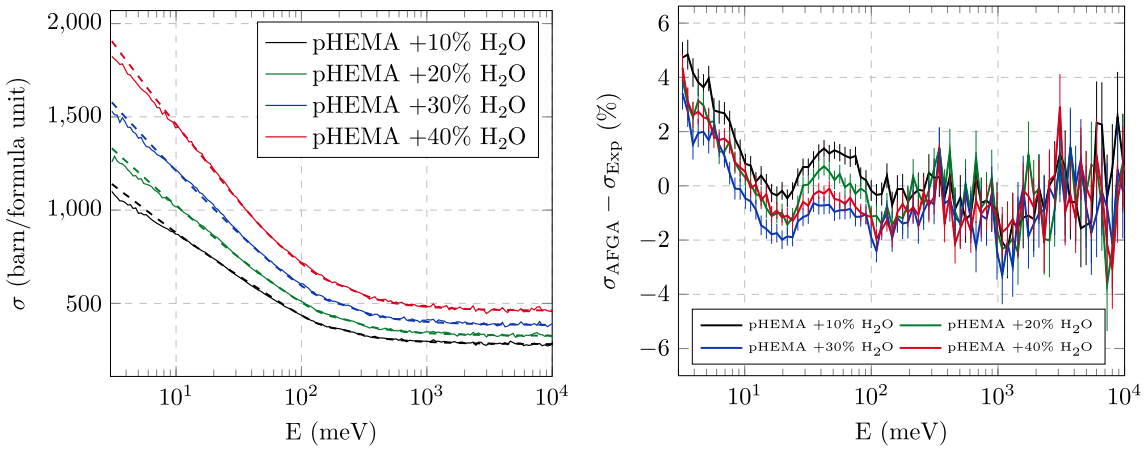

Fig. 2 Total cross section of pHEMA at different hydration levels (left panel) as a function of the incident neutron energy. Experimental data and modeling are provided as solid and dashed lines, respectively. The relative differences between the model and experimental total scattering cross section of pHEMA at different hydration levels are provided in the right panel

3 Results and discussion

The experimental results of the neutron transmission experiments are reported in Fig. 2. In particular, the left panel shows the total scattering cross section per formula unit of the monomer, according to Table 1. Data are provided for all samples at different hydration levels, and they are compared with our phenomenological modeling calculated by combining a polymer contribution using AFGA and a bulk water contribution from the CAB model by Marquez-Damian et al. [26–28]. One can appreciate a very good agreement between the experimental data and our phenomenological model over a wide range spanning about four decades of incident neutron energy. A detailed analysis of the differences between experimental spectra and modeling is provided in the right panel of Fig. 2. Despite the simplicity of our phenomenological model, the relative difference is within 2% over most of the range of incident neutron energies investigated, rising to about 4% at very low neutron energies of few meV. Such agreement supports the validity of AFGA in modeling polymers and composite materials and the level of accuracy that the approximation can reach. It is worth noting that our phenomenological model has no free parameters and that it was not fitted to the experimental data. The only input parameters in the phenomenological model were the functional group composition of the polymer and the amount of adsorbed water therein.

While the agreement between experimental data and the model is quite satisfactory at this stage, a detailed look at the right panel of Fig. 3 may provide additional information on the hydrogen dynamics in the system. The spectra in Fig. 3 (right) feature two main regions where the differences seem to be structured. First, below about 10 meV, the modeling systematically overestimates the experimental data (beyond the experimental error bars). Such a difference can be explained by considering that the model for bulk water used here is obtained by convolution of a vibrational density of states for water and a contribution related to the stochastic

Table 1 Main physical properties of a series of materials used as phantoms in neutron dosimetry

Material	Formula unit	Mass (a.m.u.)	Density (g/cm^3)	Hydrogen content (w%)	State phase
Water	H_2O	18.014	1	11.18	Liquid
Polymethyl methacrylate (PMMA)	$(C_5H_8O_2)$	100.115	1.18	8.05	Solid
Polyhydroxyethyl methacrylate (pHEMA)	$(C_6H_{10}O_3)$	130.14	1.15	7.74	Solid
pHEMA+10w% H_2O	$(C_6H_{10}O_3)$ + 0.80 (H_2O)	144.60	0.75	8.08	Hard gel
pHEMA+ 20w% H_2O	$(C_6H_{10}O_3)$ + 1.80(H_2O)	162.67	0.85	8.43	Hard gel
pHEMA+ 30w% H_2O	$(C_6H_{10}O_3)$ + 3.09(H_2O)	185.91	0.96	8.77	Gel
pHEMA+ 40w% H_2O	$(C_6H_{10}O_3)$ + 4.82(H_2O)	216.90	1.06	9.12	Gel
Polyethylene (PE)	(C_2H_4)	28.05	0.88-0.96	14.37	Solid
Brain tissue [ICRU 44]	–	–	–	10.7	–
Tissue approximation [ICRU 44]	$(C_5H_{40}O_{18}N)$	402.35	–	10.0	–
Polycarbonate (PC)	$(C_{16}H_{18}O_5)$	290.31	1.20	6.24	Solid

diffusion motions of the rigid molecule [27]. From the physical point of view, such a description may hardly represent adsorbed water molecules within the polymer, whose diffusion motions are expected to be largely suppressed by the interaction with the polymer itself. pHEMA/water systems at the same water content have been recently investigated in the μeV regime by QENS, highlighting the effect hydration and chemical nature of the hydrogel have on the polymer dynamics and water relaxation [31]. A second energy region which suggests a structured difference (although within the experimental uncertainties) is the one between about 30 and 90 meV. Here, the spectra corresponding to different hydration levels seem to spread, with the data from the polymer at the lowest hydration level (10 w%) being systematically positive. This energy region is generally associated with the librational modes in water. Similarly to the discussion about water diffusion, one can expect that the H_2O molecule adsorbed within the polymer will feature intermolecular and hydrogen-bonding interactions that are likely to shift the position of the librational modes with respect to the bulk. Such a shift would, in turn, modify the total scattering cross section, similarly to the difference that can be observed between water and ice [32].

Figure 3 (left panel) shows the mass attenuation factor of pHEMA (at 10 w% and 40 w% hydration levels) and PMMA as modeled within the AFGA. The right panel shows the relative differences of pHEMA at 10 w% and 40 w% hydration levels with respect to PMMA (dashed lines), as well as the differences between the experimental data of pHEMA at the same hydration levels and the model curve for PMMA (solid lines). In the case of the pHEMA at 10 w% hydration level, one can notice that the differences with respect to PMMA are relatively small and oscillate around 0 barn. As reported in Table 1, the hydrogen mass content is approximately the same between pHEMA+10 w%H_2O and PMMA (8.08 w% and 8.05 w%, respectively). On the other hand, one can notice significant differences, up to 10%, between pHEMA+40 w%H_2O and PMMA. The difference is not constant in energy, as the two polymers feature different hydrogen dynamics, as expected. DSC investigations of pHEMA hydrogels evidenced the presence of free water only at water contents higher than 20 w% (i.e., when the number of water molecules per HEMA hydroxyl group surpasses the value of 2) [31]. As reported in Table 1, pHEMA at the highest hydration level (40 w%) has a hydrogen content (9.12 w%) more similar to the one found in the human body (10.0 w% according to ICRU 44). Therefore, the use of pHEMA at high hydration levels as a phantom material is expected to be more representative of the average neutron attenuation properties of the human body as opposed to the largely used PMMA, and one can estimate the effect on the dose calculation as of the same order as the differences in Fig. 3 (right), i.e., between 5% and 10%. The discrepancies between theoretical and experimental curves below 10 meV in Fig. 3 (right), as discussed before, are likely related to having used a model for bulk water not representing the suppression of diffusive motion that water molecules experience when adsorbed within the polymer. Similarly, the structured difference attributed to librational modes can be appreciated between about 30 and 90 meV.

From a practical point of view, the use of pHEMA hydrogels as a material for dosimetric phantoms has pros and cons. On the one hand, being a gel, it can be used to obtain non-standard phantom geometries, with more flexibility with respect to solid materials such as PMMA or liquid materials such as the TE from [7, 8]. Moreover, the pHEMA hydrogels may be prepared to include nitrogen-containing polymers such as polyvinylpyrrolidone (PVP) [33]. This would be an additional step in obtaining a

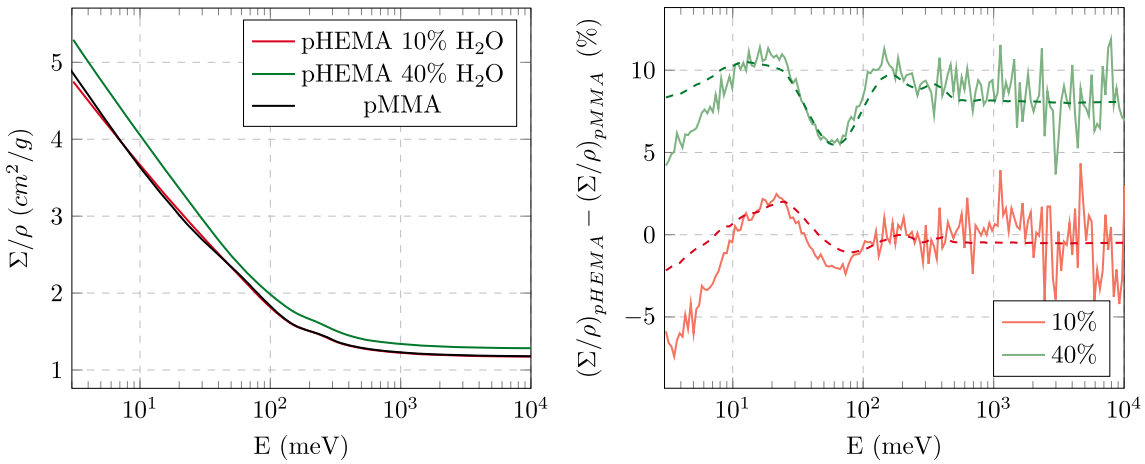

Fig. 3 Model mass attenuation factor of pHEMA at 10 w% and 40 w% hydration levels compared to the one of PMMA (left panel). The right panel shows the relative differences of pHEMA at 10 w% and 40 w% hydration levels with respect to PMMA

phantom material able to reproduce the dose related to neutron absorption in nitrogen, resulting in the emission of protons. On the other hand, a possible drawback in the use of this material is related to the stability of its hydration level. Phantoms composed of pHEMA would require some sort of external sealing, which is, however, also a requirement for liquid phantoms based on TE recipes [8].

4 Conclusions

We have presented a characterization of the neutron attenuation properties of pHEMA hydrogels at different hydration levels between 10 and 40 w% in mass based on neutron transmission experiments and theoretical modeling based on the Average Functional Group Approximation (AFGA). Our results show that phenomenological modeling can reproduce the total cross section of pHEMA very well over a broad energy range of incident neutrons, specifically at thermal energies. We have shown how, by tuning the amount of water in the polymer gel, one can obtain an attenuation coefficient which is approximately the same as the one of PMMA, a standard material used for dosimetric phantoms, or which approaches the neutron attenuation properties expected for the human body.

This was the first step in moving from standard phantoms to new and more complex materials, which may be more representative of the human body in the case of neutron irradiation and dose calculation. In particular, pHEMA can be mixed with nitrogen-containing polymers, thus allowing the inclusion of the contribution to the total dose from neutron absorption in nitrogen—an element not contained in standard phantom materials such as PMMA, water or Polyethylene, yet responsible for a large contribution to the total dose.

Finally, we have further benchmarked the validity of AFGA as a phenomenological yet accurate tool to reproduce neutron cross sections of polymers and complex molecular systems, thus confirming its suitability for use in patient-specific “personalized medicine” approaches.

Acknowledgements The authors gratefully acknowledge the support of the ISIS@MACH ITALIA Research Infrastructure, the hub of ISIS Neutron and Muon Source (UK), [MUR official registry U. 0008642.28-05-2020—16th April 2020]. The financial support from the Consiglio Nazionale delle Ricerche within the CNR-STFC Grant Agreement [No. 2021-2027] concerning collaboration in scientific research at the ISIS (UK) of STFC, is gratefully acknowledged. The STFC Rutherford Appleton Laboratory is thanked for access to neutron beam facilities. EF and TG acknowledge CSGI for partial financial support.

Funding Open access funding provided by Università degli Studi di Roma Tor Vergata within the CRUI-CARE Agreement.

Data Availability Statement This manuscript has associated data in a data repository. [Authors’ comment: The code related to the definition of the materials and the experimental data can be provided upon reasonable request].

Declarations

Conflict of interest We declare no Conflict of interest.

References

1. INTERNATIONAL ATOMIC ENERGY AGENCY, (IAEA). Advances in Boron Neutron Capture Therapy,(2023)
2. G. Romanelli, D. Onorati, P. Ulpiani, S. Cancelli, E. Perelli-Cippo, J.I.M. Damián, S.C. Capelli, G. Croci, A. Muraro, M. Tardocchi, G. Gorini, C. Andreani, R. Senesi, Thermal neutron cross sections of amino acids from average contributions of functional groups. J. Phys. Condens. Matter **33**, 285901 (2021)
3. H.B. Liu, D.D. Greenberg, J. Capala, F.J. Wheeler, An improved neutron collimator for brain tumor irradiations in clinical boron neutron capture therapy. Med. Phys. **23**, 2051–2060 (1996)
4. C.N. Culbertson, S. Green, A.J. Mason, D. Picton, G. Baugh, R.P. Hugtenburg, Z. Yin, M.C. Scott, J.M. Nelson, In-phantom characterisation studies at the Birmingham Accelerator-Generated epithermal Neutron Source (BAGINS) BNCT facility. Appl. Radiat. Isot. **61**, 733–738 (2004)
5. T. Tsukamoto, H. Tanaka, H. Yoshinaga, T. Mitsumoto, A. Maruhashi, K. Ono, Y. Sakurai, A phantom experiment for the evaluation of whole body exposure during BNCT using cyclotron-based epithermal neutron source (C-BENS). Appl. Radiat. Isot. **69**, 1830–1833 (2011)
6. Y. Sakurai, H. Tanaka, N. Kondo, Y. Kinashi, M. Suzuki, S. Masunaga, K. Ono, A. Maruhashi, Development of a dual phantom technique for measuring the fast neutron component of dose in boron neutron capture therapy. Med. Phys. **42**, 6651–6657 (2015)
7. C.P. Raaijmakers, E.L. Nottelman, B.J. Mijnheer, Phantom materials for boron neutron capture therapy. Phys. Med. Biol. **45**, 2353–2361 (2000)
8. ICRU Report 44. Tissue Substitutes in Radiation Dosimetry and Measurement, (1989)
9. T. Seppälä, J. Vähätalo, I. Auterinen, A. Kosunen, D.W. Nigg, F.J. Wheeler, S. Savolainen, Modelling of brain tissue substitutes for phantom materials in neutron capture therapy (NCT) dosimetry. RADIAT. PH. C. **55**, 239–246 (1999)
10. P.E. Tsai, Y.H. Liu, C.K. Huang, H.M. Liu, S.H. Jiang, Neutron flux mapping inside a cubic and a head PMMA phantom using indirect neutron radiography. Appl. Radiat. Isot. **67**, 190–194 (2009)
11. Y.C. Lin, Y.H. Liu, S.H. Jiang, H.M. Liu, W.T. Chou, The refinement of dose assessment of the THOR BNCT beam. Appl. Radiat. Isot. **69**, 1834–1837 (2011)
12. M.C. Hsiao, S.H. Jiang, In-phantom neutron dose measurement using Gafchromic film dosimeter for QA of BNCT beams. Appl. Radiat. Isot. **143**, 79–86 (2019)
13. W.C. Tsai, Z.Y. Yang, S.C. Lee, S.H. Jiang, Measurement of gamma-ray dose and neutron activation in BNCT beams using TLD-200. Appl. Radiat. Isot. **162**, 109146 (2020)
14. J.B. Smathers, V.A. Otte, A.R. Smith, P.R. Almond, F.H. Attix, J.J. Spokas, W.M. Quam, L.J. Goodman, Composition of A-150 tissue-equivalent plastic. Med. Phys. **4**, 74–77 (1977)
15. J. Burmeister, C. Kota, R.L. Maughan, J.J. Spokas, J.A. Coderre, R. Ma, L. Wielopolski, A conducting plastic simulating brain tissue. Med. Phys. **27**, 2560–2564 (2000)
16. S. Dowdell, B. Clasie, A. Wroe, S. Guatelli, P. Metcalfe, R. Schulte, A. Rosenfeld, Tissue equivalency of phantom materials for neutron dosimetry in proton therapy. Med. Phys. **36**, 5412–5419 (2009)
17. J. Mayers, J. Tomkinson, T. Abdul-Redah, W.G. Stirling, C. Andreani, R. Senesi, M. Nardone, D. Colognesi, E. Degiorgi, VESUVIO - the double difference inverse geometry spectrometer at ISIS. Phys. B **350**, 659–662 (2004)
18. R. Senesi, A. Pietropaolo, C. Andreani, Constant-q data representation in neutron compton scattering on the vesuvio spectrometer. Nucl. Inst. Methods Phys. Res. A **594**, 244–252 (2008)
19. G. Romanelli, M. Krzystyniak, R. Senesi, D. Raspino, J. Boxall, D. Pooley, S. Moorby, E. Schooneveld, N. Rhodes, C. Andreani, F. Fernandez-Alonso, Characterisation of the incident beam and current diffraction capabilities on the VESUVIO spectrometer. Meas. S. and T. **28**, 095501 (2017)
20. J.I. Robledo, J. Dawidowski, J.I.M. Damián, G. Škoro, C. Bovo, G. Romanelli, Measurement of neutron total cross sections at the VESUVIO spectrometer. Nucl. Inst. Meth. **971**, 164096 (2020)
21. O. Arnold, J.C. Bilheux, J.M. Borreguero, A. Buts, S.I. Campbell,L. Chapon, M. Doucet, N. Draper, R. Ferraz Leal, M.A.Gigg, V.E. Lynch,A.Markvardsen, D.J.Mikkelson, R.L.Mikkelson, R.Miller,K.Palmen, P.Parker, G.Passos, T.G.Perring, P.F.Peterson,S.Ren, M.A.Reuter, A.T.Savici, J.W.Taylor, R.J.Taylor,R.Tolchenov, W.Zhou, J.Zikovsky, Mantid-data analysis andvisualization package for neutron scattering and muon SR experiments. Nuclear Instruments and Methods in Physics Research Section A: Accelerators, Spectrometers, Detectors and AssociatedEquipment 764, 156–166 (2014) https://doi.org/10.1016/j.nima.2014.07.029
22. V.F. Sears, Neutron scattering lengths and cross sections. Neutron News **3**(3), 26–37 (1992). https://doi.org/10.1080/10448639208218770
23. G. Romanelli, M. Simoni, E. Preziosi, J.I. Marquez-Damian, C. Andreani, R. Senesi, Neutron thermal cross sections of 3D-printing organic polymers using the Average Functional Group Approximation. EPJ Web of Con. **284**, 17010 (2023)
24. G. Romanelli, S. Capuani, D. Onorati, P. Ulpiani, E. Preziosi, C. Andreani, R. Senesi, Fluorinated borono-phenylalanine for optimizing bnct: Enhancing boron absorption against hydrogen scattering for thermal neutrons. Med. Phys. **51**(1), 439–446 (2024). https://doi.org/10.1002/mp.16802
25. X. Cai, T. Kittelmann, Ncrystal: A library for thermal neutron transport. Comput. Phys. Commun. **246**, 106851 (2020)
26. Ncrystal-H2O [Online]. https://raw.githubusercontent.com/wiki/mctools/ncrystal/datalib/LiquidWaterHosub42o/sub4O_T293.6K.ncmat
27. J. Màrquez-Damiàn, J. Granada, D. Malaspina, CAB models for water: A new evaluation of the thermal neutron scattering laws for light and heavy water in ENDF-6 format. Ann. Nucl. Energy **65**, 280–289 (2014)
28. J.I. Marquez-Damian, D.C. Malaspina, J.R. Granada, Vibrational spectra of light and heavy water with application to neutron cross section calculations. J. Chem. Phys. **139**, 024504 (2013)
29. K. Yoshida, C. Wakai, N. Matubayasi, M. Nakahara, A new high-temperature multinuclear-magnetic-resonance probe and the self-diffusion of light and heavy water in sub- and supercritical conditions. J. Chem. Phys. **123**, 164506 (2005)
30. R. Mills, Self-diffusion in normal and heavy water in the range 1–45 deg. J. Phys. Chem. **77**, 685–688 (1973)
31. D. Noferini, A. Faraone, M. Rossi, E. Mamontov, E. Fratini, P. Baglioni, Disentangling polymer network and hydration water dynamics in polyhydroxyethyl methacrylate physical and chemical hydrogels. J. Phys. Chem. C. **123**, 19183–19194 (2019). https://doi.org/10.1021/acs.jpcc.9b04212
32. C. Andreani, R. Senesi, M. Krzystyniak, G. Romanelli, F. Fernandez-Alonso, Experimental studies of nuclear quantum effects in condensed matter: the case of water. Riv. Nuovo Cim. **41**, 291–340 (2018)
33. J.A.L. Domingues, N. Bonelli, R. Giorgi, E. Fratini, F. Gorel, P. Baglioni, Innovative hydrogels based on semi-interpenetrating p(HEMA)/PVP networks for the cleaning of water-sensitive cultural heritage artifacts. J. Langmuir **29**, 2746–2755 (2013)